

Correlated Electronic Structure and Density-Wave Gap in Trilayer

Nickelate $\text{La}_4\text{Ni}_3\text{O}_{10}$

X. Du¹, Y. D. Li¹, Y. T. Cao^{2,3}, C. Y. Pei⁴, M. X. Zhang⁴, W. X. Zhao¹, K. Y. Zhai¹, R. Z. Xu¹, Z. K. Liu^{4,5}, Z. W. Li², J. K. Zhao³, G. Li⁴, Y. L. Chen^{4,5,6†}, Y. P. Qi^{4,5,7†}, H. J. Guo^{3†}, and L. X. Yang^{1,8†}

¹State Key Laboratory of Low Dimensional Quantum Physics, Department of Physics, Tsinghua University, Beijing 100084, China

²School of Physical Science and Technology, Lanzhou University, Lanzhou 730000, China

³Songshan Lake Materials Laboratory, Dongguan, Guangdong 523808, China

⁴School of Physical Science and Technology, ShanghaiTech University, Shanghai 201210, China

⁵ShanghaiTech Laboratory for Topological Physics, Shanghai 200031, China

⁶Department of Physics, Clarendon Laboratory, University of Oxford, Parks Road, Oxford OX1 3PU, UK

⁷Shanghai Key Laboratory of High-resolution Electron Microscopy, ShanghaiTech University, Shanghai 201210, China

⁸Frontier Science Center for Quantum Information, Beijing 100084, China

Emails: LXY: lxyang@tsinghua.edu.cn; YLC: yulin.chen@physics.ox.ac.uk; YPQ: qiyp@shanghaitech.edu.cn; HJG: hjguo@sslaborg.org.cn

The discovery of pressurized superconductivity at 80 K in $\text{La}_3\text{Ni}_2\text{O}_7$ officially brings nickelates into the family of high-temperature superconductors, which gives rise to not only new insights but also mysteries in the strongly correlated superconductivity. More recently, the sibling compound $\text{La}_4\text{Ni}_3\text{O}_{10}$ was also shown to be superconducting below about 25 K under pressure, further boosting the popularity of nickelates in the Ruddlesden-Popper phase. In this study, combining high-resolution angle-resolved photoemission spectroscopy and *ab initio* calculation, we systematically investigate the electronic structures of $\text{La}_4\text{Ni}_3\text{O}_{10}$ at ambient pressure. We reveal a high resemblance of $\text{La}_4\text{Ni}_3\text{O}_{10}$ with $\text{La}_3\text{Ni}_2\text{O}_7$ in the orbital-dependent fermiology and electronic structure, suggesting a similar electronic correlation between the two compounds. The temperature-dependent measurements imply an orbital-dependent energy gap related to the density-wave transition in $\text{La}_4\text{Ni}_3\text{O}_{10}$. By comparing the theoretical pressure-dependent electronic structure, clues about the superconducting high-pressure phase can be deduced from the ambient measurements, providing crucial information for deciphering the unconventional superconductivity in nickelates.

Since its discovery, high-temperature superconductivity (HTSC) in cuprates remains one of the most challenging mysteries in condensed matter physics [1,2]. To advance the understanding of this problem, it is highly pursued to search for analogs to cuprates with similar superconducting and normal-state properties. Nickelates are believed to be promising candidates for high-temperature superconductors with strong electronic correlation. Unconventional superconductivity has been discovered in infinite-layer [3-5] and quintuple-layer [6] nickelates, in which $3d$ electrons of Ni dominate the electronic states near the Fermi level (E_F). In particular, Ni^{+} exhibits an effective electronic configuration of $3d^9$, strikingly resembling Cu^{2+} in cuprates [7,8]. Moreover, the electronic correlation likewise plays a pivotal role in the electronic structure of nickelate superconductors [9]. Such similitude makes nickelates an attractive platform for exploring HTSC. However, the synthesis of these nickelates is challenging and the superconductivity is realized only in thin films with T_c far below the criterion of HTSC regardless of the application of pressure [3,5].

Recently, HTSC with T_c up to 80 K was discovered in $La_3Ni_2O_7$ bulk compound under pressures between 14.0 GPa and 43.5 GPa [10-13]. Likewise, the signature of superconductivity under pressure with the maximum T_c between 20 K and 30 K has been observed in the sister compound $La_4Ni_3O_{10}$ [14-16]. With the chemical formula of $La_{n+1}Ni_nO_{3n+1}$, both compounds belong to the Ruddlesden-Popper (RP) phase, which can be viewed as the parent phase of the infinite-layer and quintuple-layer nickelates. They exhibit extraordinary properties at ambient pressure, including orbital-dependent electronic correlation, non-Fermi liquid behavior, and the interplay with density-wave states [12,17-19]. Many theoretical understandings of the electronic structure and superconductivity of the bilayer and trilayer nickelates have been proposed with the focus on the correlated electronic structure of the $d_{x^2-y^2}$ and d_{z^2} orbitals [20-33]. While it is challenging to experimentally investigate the electronic structure at high pressure, the experiments at ambient pressure will provide crucial information. Previous angle-resolved photoemission spectroscopy (ARPES) measurements have revealed the basic electronic structure and electronic correlation in $La_3Ni_2O_7$ [17,34] and $La_4Ni_3O_{10}$ [35], with more details awaiting further experimental exploration. Furthermore, a comparing investigation of the electronic structures of the bilayer and trilayer nickelates will offer important insights into their normal-state and superconducting properties.

In this work, we systematically investigate the electronic structure of $La_4Ni_3O_{10}$ at ambient pressure

with high-resolution ARPES in comparison to $\text{La}_3\text{Ni}_2\text{O}_7$ and explore the effect of pressure with *ab initio* calculation. The experimental and calculated band structure of $\text{La}_4\text{Ni}_3\text{O}_{10}$ is very similar to that of $\text{La}_3\text{Ni}_2\text{O}_7$. The low-energy electronic structure is dominated by Ni $3d_{x^2-y^2}$ and $3d_{z^2}$ orbitals. In particular, the $3d_{z^2}$ orbitals form flat bands near E_F , which contribute significantly to the density of states (DOS). At high pressure, our *ab initio* calculation suggests that the bandwidth increases by about 20%, while the band dispersions near E_F show a minor change. Furthermore, in the energy bands with $d_{x^2-y^2}$ and d_{z^2} hybridization, we observe a gap showing Bardeen-Cooper-Shrieffer (BCS) type temperature-dependence below the charge/spin-density wave (CDW/SDW) transition temperature of $\text{La}_4\text{Ni}_3\text{O}_{10}$. More interestingly, the gap amplitude shows an anisotropy that is correlated with the strength of the hybridization between the $d_{x^2-y^2}$ and d_{z^2} orbitals. Our comparing study of the bilayer and trilayer nickelates will help construct a unified understanding of the normal-state and superconducting picture of the unconventional HTSC in nickelates of the RP phase.

The crystal structures of $\text{La}_4\text{Ni}_3\text{O}_{10}$ and $\text{La}_3\text{Ni}_2\text{O}_7$ are shown in Figs. 1(a) and 1(b), respectively. As sister compounds in the RP phase, both materials feature layered structures made of corner-sharing Ni-O octahedron layers [10,36]. In contrast to the equivalent Ni-O layers in $\text{La}_3\text{Ni}_2\text{O}_7$, $\text{La}_4\text{Ni}_3\text{O}_{10}$ harbors two sets of inequivalent Ni-O layers. At ambient pressure, the vertical axes of the octahedrons cant by an angle of about 8° (6°) with respect to the c axis in $\text{La}_4\text{Ni}_3\text{O}_{10}$ ($\text{La}_3\text{Ni}_2\text{O}_7$). A pressure above about 13 GPa aligns the axes and changes the crystal symmetry, which is believed to be crucial for the superconductivity [36]. Laue measurement [Fig. 1(c)] of the (001) surface confirms the high quality of the $\text{La}_4\text{Ni}_3\text{O}_{10}$ crystals used in our work. The magnetic susceptibility decreases with decreasing temperature followed by a sudden drop (enhancement) of the in-plane (out-of-plane) component near 132 K [Fig. 1(c)]. Correspondingly, the specific heat shows a cusp near 132 K [Fig. 1(d)], in nice agreement with previous reports [37,38], which has been ascribed to an intertwined density-wave transition with both charge and magnetic characters [39].

Figures 2 (a-d) present the measured band structure of $\text{La}_4\text{Ni}_3\text{O}_{10}$. As shown in Fig. 2(a), the Fermi surface (FS) is mainly made up of three sets of bands. The α and β bands compose a nearly-circular sheet and a larger rounded-square sheet around the $\bar{\Gamma}$ point, respectively, which are better visualized in the laser-ARPES data in Fig. 2(b). Along the $\bar{\Gamma}\bar{X}$ direction [Fig. 2(c)], the α and β bands are

nearly degenerate, while the γ band approaches E_F with a flat band top. The flat γ band is better resolved along the $\bar{\Gamma}\bar{S}$ direction in the second Brillouin zone [the red dashed line in Fig. 2(a), also see Supplemental Materials [40]]. The overall electronic structure is in good agreement with the previous ARPES experiment [14,35].

In Figs. 2(e-h) we compare the band structures of $\text{La}_4\text{Ni}_3\text{O}_{10}$ and $\text{La}_3\text{Ni}_2\text{O}_7$. Despite their distinct number of Ni-O octahedron layers, both their Fermiology and energy dispersions are analogous (more data are presented in Supplemental Materials [40]). In particular, both FSs measured at 98 eV are consisted of parallel FS sheets with strong spectral weight, providing an electronic basis for the FS nesting. The observed similarity between the electronic structures of $\text{La}_4\text{Ni}_3\text{O}_{10}$ and $\text{La}_3\text{Ni}_2\text{O}_7$ is, however, out of the expectation since the inequivalent Ni-O layers in $\text{La}_4\text{Ni}_3\text{O}_{10}$ are supposed to contribute additional bands. The absence of additional bands compared to $\text{La}_3\text{Ni}_2\text{O}_7$ might be due to the matrix element effect or a delicate band-splitting issue [35]. Indeed, the experimental electronic structure of a $\text{La}_5\text{Ni}_4\text{O}_{13}$ thin film, another member of the RP phase nickelates, also resembles those of the two materials in our study [41,42].

To further comprehend the electronic structure of $\text{La}_4\text{Ni}_3\text{O}_{10}$, we perform detailed band structure calculations in Fig. 3 (and a comparison with $\text{La}_3\text{Ni}_2\text{O}_7$ in Supplemental Materials [40]). Figure 3(a) shows the *ab initio* calculation of the band structure projected onto atomic orbitals (Supplemental Materials [40]). The bands near E_F are mainly composed of Ni $3d$ orbitals hybridized with O $2p$ orbitals. Due to the crystal-field splitting, the e_g bands locate near E_F and separate from the t_{2g} bands in energy. The trilayer structure induces three sets of energy bands, as can be better visualized near the Γ and Z points. Due to the inter-layer coupling, the d_{z^2} -orbital derived bands split into bonding, non-bonding, and anti-bonding bands with distinct energies, while the in-plane $d_{x^2-y^2}$ -orbital derived bands show a much smaller splitting.

Based on these characteristics, we carry out Wannier orbital calculation, which yields two sets of Wannier orbitals involving Ni $3d_{z^2} - \text{O } 2p_z$ and Ni $3d_{x^2-y^2} - \text{O } 2p_{x/y}$ hybridized atomic orbitals, respectively [Fig. 3(b)]. By comparing with the experimental band structure, we determine the renormalization factors of the d_{z^2} and $d_{x^2-y^2}$ orbitals to be 5 and 3, respectively (Supplemental Materials [40]), which reflects the more-localized nature of the d_{z^2} orbitals [27]. We also calculate the FS with momentum-dependent weight of atomic orbitals as shown in Fig. 3(c). The calculated

and experimental results agree well if the $d_{z^2}/d_{x^2-y^2}$ -derived bonding bands and the $d_{x^2-y^2}$ -derived anti-bonding bands are considered [35] (Supplemental Materials [40]). It is noteworthy that the α and β bands are mixtures of the two e_g orbitals (d_{z^2} and $d_{x^2-y^2}$), with a pure $d_{x^2-y^2}$ character only along the ΓX direction. By contrast, the γ band consists exclusively of d_{z^2} character. The electronic structure is also calculated for the pressurized phase at 30.5 GPa [Figs. 3(d-f)] [36]. As shown in Fig. 3(d), the overall band structure of the high-pressure phase coincides with that of the ambient phase. We note that the bandwidth increases by about 20%, while the band dispersions near E_F barely change with increasing pressure, except that the overlap and hybridization between the bonding and non-bonding d_{z^2} bands reduce near Γ but increase near Z . Due to the alignment of the Ni-O octahedrons under pressure, the orbital components of the Wannier orbitals appear to be unmixed, forming inter- and intra-layer σ bonds, which are analogous to the situation in $\text{La}_3\text{Ni}_2\text{O}_7$ and favor the pressurized superconductivity [10]. In the FS, both the nearly-circular α -sheet and the large round-square-like β -sheet show minor change, while the small hole pocket from the hybridization between the bonding and non-bonding d_{z^2} bands evolves into two small anisotropic pockets at Γ . It is worth noting that the small overlap between the bonding and non-bonding d_{z^2} bands in the calculation may lead to the mutable topology of FS with pressure and electron doping. Figure 4 presents the temperature-dependent laser-ARPES spectra along the $\bar{\Gamma}\bar{S}$ and $\bar{\Gamma}\bar{X}$ directions [dashed arrows in Fig. 2(b)], respectively. As shown in Fig. 4(a), the spectral weight of the α band reduces as approaching E_F without a quasiparticle peak at low temperatures along the $\bar{\Gamma}\bar{S}$ direction. With increasing temperature, the spectral weight near E_F increases [Figs. 4(b-d)] and the leading edge of the energy distribution curves (EDCs) gradually shifts towards E_F [Figs. 4(e)], suggesting an energy gap at low temperatures. Figure 4(f) summarizes the leading-edge position as a function of the temperature, which shows the development of the gap below 130 K, consistent with the density-wave transition. The saturated gap at the lowest temperature Δ_0 is about 12 meV, smaller than the previously reported value of 20 meV determined by the peak position in the flat band [35]. The reduced gap is estimated to be $\frac{2\Delta_0}{k_B T} \approx 2.1$, less than the mean-field expectation of 3.52, suggesting a relatively weak energy condensation of the density-wave state in $\text{La}_4\text{Ni}_3\text{O}_{10}$ [43]. The situation along the $\bar{\Gamma}\bar{X}$ direction is more complex due to the two nearly-degenerate bands

crossing E_F [Figs. 4(g-j)]. While the α band likewise shows a reduced spectral weight at low temperatures, the β band develops a peak below 130 K, as better visualized in the temperature-dependent EDCs in Figs. 4(k) and (l). Moreover, the leading edge of the EDCs at k_F^α along $\bar{\Gamma}\bar{X}$ shows a negligible shift compared to the $\bar{\Gamma}\bar{S}$ direction. This contrasting behavior along the two directions indicates an anisotropic CDW gap in the α band of $\text{La}_4\text{Ni}_3\text{O}_{10}$ at ambient pressure [39]. This behavior is likely related to the hybridization between the $d_{x^2-y^2}$ and d_{z^2} orbitals, which is strongest along the $\bar{\Gamma}\bar{S}$ direction but becomes negligible along $\bar{\Gamma}\bar{X}$ [Fig. 3(c)]. At k_F^β , we observe a small leading-edge shift of about 6 ± 4 meV, compared to the peak position at about -20 meV at 20 K, which was not resolved in the previous measurement [35]. For the flat γ band, no shift with temperature is observed (Supplemental Materials [40]), which is in contrast to the previous report [35], but similar to the case in $\text{La}_3\text{Ni}_2\text{O}_7$ [17].

Our measurements of the ambient phase of the two compounds provide abundant information for understanding the novel normal-state properties and deciphering the unconventional superconductivity of RP-phase nickelates at high pressure. Firstly, the experimental low-energy electronic structures of the two compounds are very alike, which fit well to the calculated bands (Supplemental Materials [40]). This surprising observation suggests a similar electronic basis for the superconductivity in the two materials [44]. Secondly, the nice agreement between the calculated results and experiments at ambient pressure with an orbital-dependent renormalization can possibly be extrapolated to the pressurized phases, which is a necessary ingredient in theoretical modeling. In general, our data demonstrate the more correlated nature of the d_{z^2} orbital than the $d_{x^2-y^2}$ orbital, consistent with the theoretical understanding of the distinctive correlation of the two orbitals due to electron filling [27,45,46]. Thirdly, with a flat band top near E_F , the FS sheets of the d_{z^2} bands are highly sensitive to the exact position of E_F . In $\text{La}_3\text{Ni}_2\text{O}_7$, the band is proposed to be metalized with a new pocket in the FS under pressure [10], which is believed to be important to the HTSC [47,48]. Indeed, the subtle Fermiology can conspire with the oxygen deficiency to strongly influence the electron pairing, and even spoil the HTSC of $\text{La}_3\text{Ni}_2\text{O}_7$ [32,48-50]. Finally, the sharp density-wave transition shown in the ambient phase of $\text{La}_4\text{Ni}_3\text{O}_{10}$ might compete with the superconductivity, as the electronic DOS at E_F is suppressed by the CDW transition. For $\text{La}_3\text{Ni}_2\text{O}_7$, by contrast, the phase transition seems to be weaker and more elusive [10,19,44,48], which might

be an advantage for the HTSC.

In conclusion, we systematically investigate the electronic structure of $\text{La}_4\text{Ni}_3\text{O}_{10}$ and $\text{La}_3\text{Ni}_2\text{O}_7$ at ambient pressure both experimentally and theoretically, and explore the effect of pressure theoretically. The high similarity in the electronic structure of these two materials is revealed. The anisotropic energy gap related to the density-wave transition accords with the momentum distribution of the orbital components in the corresponding energy band in $\text{La}_4\text{Ni}_3\text{O}_{10}$. The nice agreement of the experimental results with the calculation after an orbital-dependent renormalization provides important hints to the exploration of HTSC in nickelates.

Acknowledgement

This work is funded by the National Key R&D Program of China (Grant No. 2022YFA1403201 and Grant No. 2022YFA1403100), the National Natural Science Foundation of China (No. 12274251, 12004270, and 52272265), and the Guangdong Basic and Applied Basic Research Foundation (Grant No. 2022B1515120020). L.X.Y. acknowledges support from the Tsinghua University Initiative Scientific Research Program and the Fund of Science and Technology on Surface Physics and Chemistry Laboratory (No. XKFZ202102). We thank the MAX IV Laboratory for the time on beamline Bloch under Proposal 20230668, and the SSRF for the time on beamline 03U under Proposal No. 2023-SSRF-PT-502880.

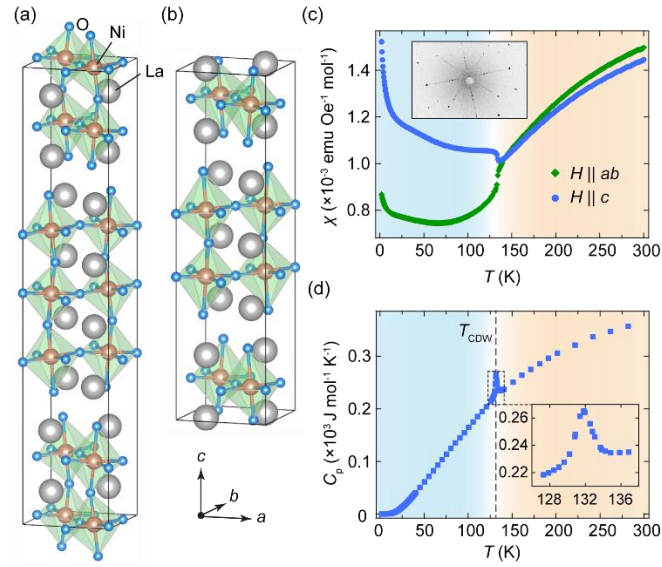


FIG. 1. (a, b) Crystal structures of $\text{La}_4\text{Ni}_3\text{O}_{10}$ (a) and $\text{La}_3\text{Ni}_2\text{O}_7$ (b) at ambient pressure. (c) Magnetic susceptibility along the ab and c directions as a function of temperature of $\text{La}_4\text{Ni}_3\text{O}_{10}$. The inset shows the Laue pattern for (001) surface. (d) Specific heat as a function of temperature of $\text{La}_4\text{Ni}_3\text{O}_{10}$. The inset highlights the cusp near 132 K.

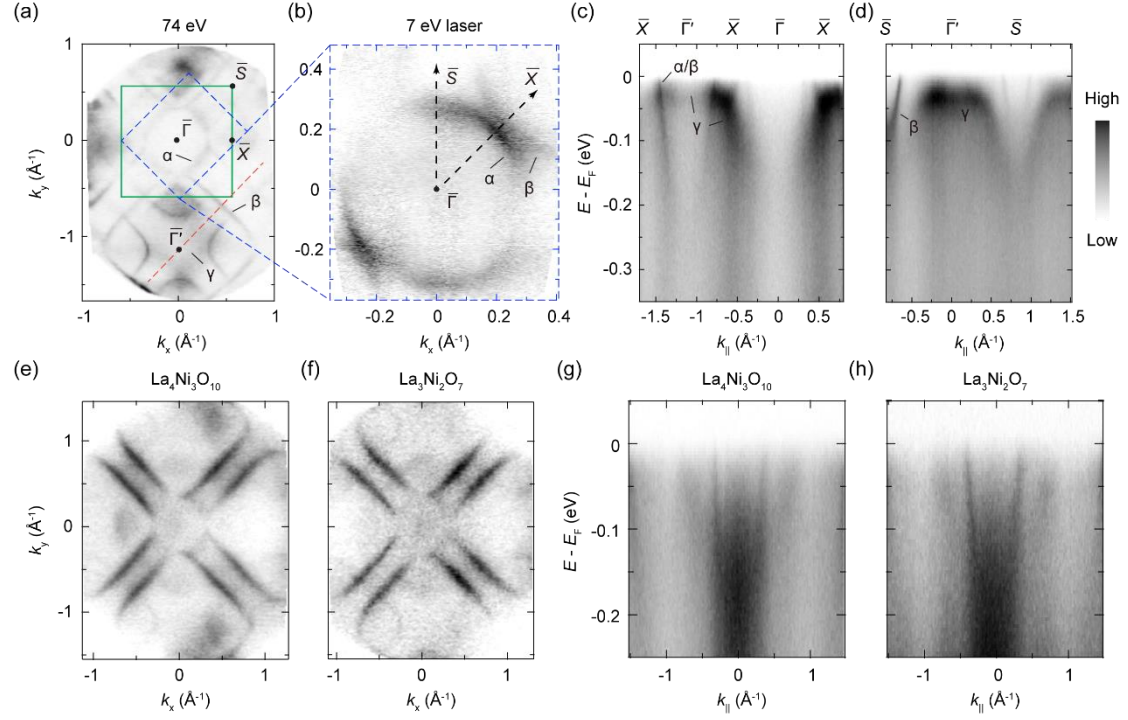


FIG. 2. (a) Experimental Fermi surface (FS) of $\text{La}_4\text{Ni}_3\text{O}_{10}$ integrated within an energy window of ± 20 meV around the Fermi level (E_F). Data were collected with 74 eV photons. The surface Brillouin zone (BZ) is overlaid as green lines. (b) FS measured with a 7-eV laser corresponding to the blue dashed area in (a). (c, d) Band dispersions along the high-symmetry directions of $\bar{\Gamma}\bar{X}$ (c) and $\bar{\Gamma}\bar{S}$ (d) measured at the photon energy of 74 eV. Data in (d) were collected with a geometry indicated by the red dashed line in (a). (e), (f) Experimental FS of $\text{La}_4\text{Ni}_3\text{O}_{10}$ and $\text{La}_3\text{Ni}_2\text{O}_7$ measured at the photon energy of 98 eV, respectively. (g, h) Band dispersions of $\text{La}_4\text{Ni}_3\text{O}_{10}$ and $\text{La}_3\text{Ni}_2\text{O}_7$ along $\bar{\Gamma}\bar{X}$ measured at the photon energy of 98 eV, respectively. Data in (b) were collected with linear-vertically polarized photons at 80 K. All other data were collected with linear-horizontally polarized photons at 20 K.

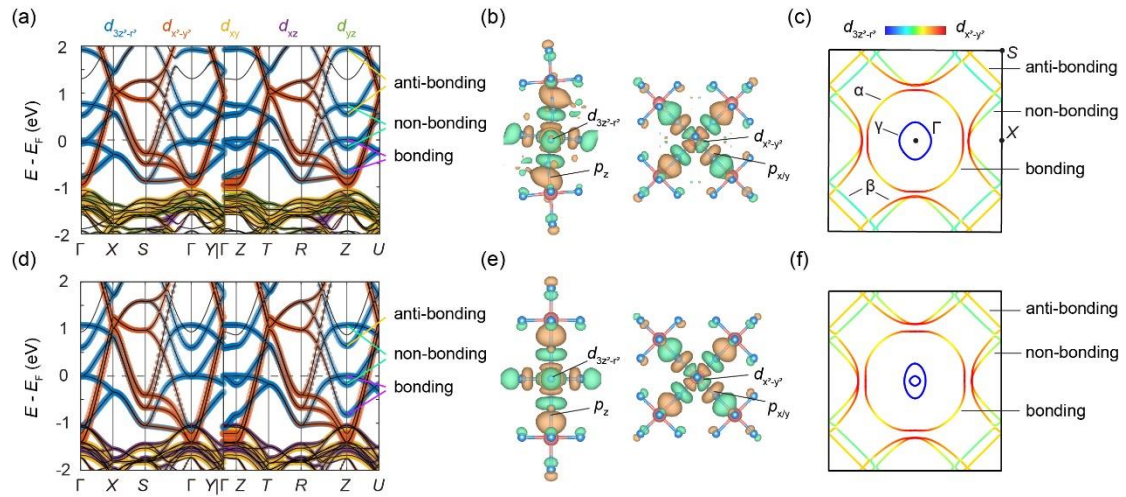


FIG. 3. (a) Calculated band structure with atomic orbital projection for the ambient phase of $\text{La}_4\text{Ni}_3\text{O}_{10}$. (b) Calculated Wannier orbital of the ambient phase showing the Ni $3d_{z^2} - 2p_z$ and Ni $3d_{x^2-y^2} - 2p_{x/y}$ hybridized atomic orbitals that are centered at Ni atoms in the middle Ni-O layers. (c) Cross-section of FS in the $k_z = 0$ plane with atomic orbital projections. (d-f) Same as those in (a-c), but for the high-pressure phase of $\text{La}_4\text{Ni}_3\text{O}_{10}$.

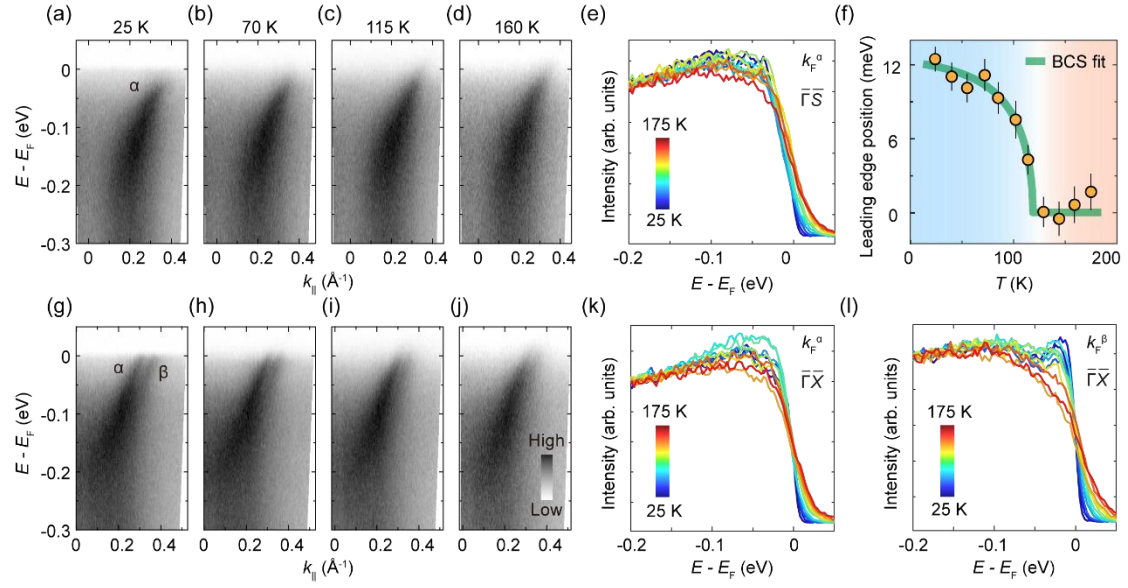


FIG. 4. (a-d) Temperature-dependent ARPES spectra of $\text{La}_4\text{Ni}_3\text{O}_{10}$ along the $\bar{\Gamma}\bar{S}$ direction. (e) The energy distribution curves (EDCs) at the Fermi momenta (k_F) at different temperatures. (f) Corresponding leading-edge positions of the EDCs. (g-j) Temperature-dependent ARPES spectra along the $\bar{\Gamma}\bar{X}$ direction. (k, l) The EDCs at k_F^α and k_F^β at different temperatures, respectively. Data in (a-f) and (g-l) were collected with linear-vertically and linear-horizontally polarized photons with 7-eV energy, respectively.

References

- [1] X. Zhou, W.-S. Lee, M. Imada, N. Trivedi, P. Phillips, H.-Y. Kee, P. Törmä, and M. Eremets, High-temperature superconductivity, *Nat. Rev. Phys.* **3**, 462 (2021).
- [2] B. Keimer, S. A. Kivelson, M. R. Norman, S. Uchida, and J. Zaanen, From quantum matter to high-temperature superconductivity in copper oxides, *Nature* **518**, 179 (2015).
- [3] D. Li, K. Lee, B. Y. Wang, M. Osada, S. Crossley, H. R. Lee, Y. Cui, Y. Hikita, and H. Y. Hwang, Superconductivity in an infinite-layer nickelate, *Nature* **572**, 624 (2019).
- [4] S. Zeng *et al.*, Superconductivity in infinite-layer nickelate $\text{La}_{1-x}\text{Ca}_x\text{NiO}_2$ thin films, *Sci. Adv.* **8**, eabl9927 (2022).
- [5] N. N. Wang *et al.*, Pressure-induced monotonic enhancement of T_c to over 30 K in superconducting

Pr_{0.82}Sr_{0.18}NiO₂ thin films, Nat. Commun. **13**, 4367 (2022).

[6] G. A. Pan *et al.*, Superconductivity in a quintuple-layer square-planar nickelate, Nat. Mater. **21**, 160 (2021).

[7] M. Hepting *et al.*, Electronic structure of the parent compound of superconducting infinite-layer nickelates, Nat. Mater. **19**, 381 (2020).

[8] H. Sakakibara, H. Usui, K. Suzuki, T. Kotani, H. Aoki, and K. Kuroki, Model Construction and a Possibility of Cupratelike Pairing in a New d⁹ Nickelate Superconductor (Nd,Sr)NiO₂, Phys. Rev. Lett. **125**, 077003 (2020).

[9] A. Kreisels, B. M. Andersen, A. T. Rømer, I. M. Eremin, and F. Lechermann, Superconducting Instabilities in Strongly Correlated Infinite-Layer Nickelates, Phys. Rev. Lett. **129**, 077002 (2022).

[10] H. Sun *et al.*, Signatures of superconductivity near 80 K in a nickelate under high pressure, Nature **621**, 493 (2023).

[11] J. Hou *et al.*, Emergence of High-Temperature Superconducting Phase in Pressurized La₃Ni₂O₇ Crystals, Chin. Phys. Lett. **40**, 117302 (2023).

[12] Y. Zhang *et al.*, High-temperature superconductivity with zero-resistance and strange metal behavior in La₃Ni₂O₇, arXiv:2307.14819 (2023).

[13] M. Zhang, C. Pei, Q. Wang, Y. Zhao, C. Li, W. Cao, S. Zhu, J. Wu, and Y. Qi, Effects of pressure and doping on Ruddlesden-Popper phases La_{n+1}Ni_nO_{3n+1}, J. Mater. Sci. Technol. **185**, 147 (2024).

[14] M. Zhang *et al.*, Superconductivity in trilayer nickelate La₄Ni₃O₁₀ under pressure, arXiv:2311.07423 (2023).

[15] Q. Li, Y.-J. Zhang, Z.-N. Xiang, Y. Zhang, X. Zhu, and H.-H. Wen, Signature of Superconductivity in Pressurized La₄Ni₃O₁₀, Chin. Phys. Lett. **41**, 017401 (2024).

[16] Y. Zhu *et al.*, Superconductivity in trilayer nickelate La₄Ni₃O₁₀ single crystals, arXiv:2311.07353 (2023).

[17] J. Yang *et al.*, Orbital-Dependent Electron Correlation in Double-Layer Nickelate La₃Ni₂O₇, Nat. Commun. **15**, 4373 (2024).

[18] Z. Liu *et al.*, Electronic correlations and energy gap in the bilayer nickelate La₃Ni₂O₇, arXiv:2307.02950 (2023).

[19] Z. Liu *et al.*, Evidence for charge and spin density waves in single crystals of La₃Ni₂O₇ and La₃Ni₂O₆, Sci. China: Phys. Mech. Astron. **66**, 217411 (2022).

- [20] Z. Luo, X. Hu, M. Wang, W. Wú, and D.-X. Yao, Bilayer Two-Orbital Model of $\text{La}_3\text{Ni}_2\text{O}_7$ under Pressure, *Phys. Rev. Lett.* **131**, 126001 (2023).
- [21] Y. Zhang, L.-F. Lin, A. Moreo, and E. Dagotto, Electronic structure, dimer physics, orbital-selective behavior, and magnetic tendencies in the bilayer nickelate superconductor $\text{La}_3\text{Ni}_2\text{O}_7$ under pressure, *Phys. Rev. B* **108**, L180510 (2023).
- [22] F. Lechermann, J. Gondolf, S. Bötzel, and I. M. Eremin, Electronic correlations and superconducting instability in $\text{La}_3\text{Ni}_2\text{O}_7$ under high pressure, *Phys. Rev. B* **108**, L201121 (2023).
- [23] Y. Cao and Y.-f. Yang, Flat bands promoted by Hund's rule coupling in the candidate double-layer high-temperature superconductor $\text{La}_3\text{Ni}_2\text{O}_7$ under high pressure, *Phys. Rev. B* **109**, L081105 (2024).
- [24] Z. Liao, L. Chen, G. Duan, Y. Wang, C. Liu, R. Yu, and Q. Si, Electron correlations and superconductivity in $\text{La}_3\text{Ni}_2\text{O}_7$ under pressure tuning, *Phys. Rev. B* **108**, 214522 (2023).
- [25] Y. Shen, M. Qin, and G.-M. Zhang, Effective Bi-Layer Model Hamiltonian and Density-Matrix Renormalization Group Study for the High- T_c Superconductivity in $\text{La}_3\text{Ni}_2\text{O}_7$ under High Pressure, *Chin. Phys. Lett.* **40**, 127401 (2023).
- [26] Y. Gu, C. Le, Z. Yang, X. Wu, and J. Hu, Effective model and pairing tendency in bilayer Ni-based superconductor $\text{La}_3\text{Ni}_2\text{O}_7$, *arXiv:2306.07275* (2023).
- [27] Y.-f. Yang, G.-M. Zhang, and F.-C. Zhang, Interlayer valence bonds and two-component theory for high- T_c superconductivity of $\text{La}_3\text{Ni}_2\text{O}_7$ under pressure, *Phys. Rev. B* **108**, L201108 (2023).
- [28] Y.-H. Tian, Y. Chen, J.-M. Wang, R.-Q. He, and Z.-Y. Lu, Correlation Effects and Concomitant Two-Orbital $s\pm$ -Wave Superconductivity in $\text{La}_3\text{Ni}_2\text{O}_7$ under High Pressure, *arXiv:2308.09698* (2023).
- [29] W. Wú, Z. Luo, D.-X. Yao, and M. Wang, Superexchange and charge transfer in the nickelate superconductor $\text{La}_3\text{Ni}_2\text{O}_7$ under pressure, *Science China Physics, Mechanics & Astronomy* **67**, *arXiv:2307.05662* (2024).
- [30] V. Christiansson, F. Petocchi, and P. Werner, Correlated Electronic Structure of $\text{La}_3\text{Ni}_2\text{O}_7$ under Pressure, *Phys. Rev. Lett.* **131**, 206501 (2023).
- [31] J.-X. Zhang, H.-K. Zhang, Y.-Z. You, and Z.-Y. Weng, Strong Pairing Originated from an Emergent Z_2 Berry Phase in $\text{La}_3\text{Ni}_2\text{O}_7$, *arXiv:2309.05726* (2023).
- [32] H. Sakakibara *et al.*, Theoretical analysis on the possibility of superconductivity in the trilayer Ruddlesden-Popper nickelate $\text{La}_4\text{Ni}_3\text{O}_{10}$ under pressure and its experimental examination: Comparison with $\text{La}_3\text{Ni}_2\text{O}_7$, *Phys. Rev. B* **109**, 144511 (2024).

- [33] H. LaBollita, V. Pardo, M. R. Norman, and A. S. Botana, Electronic structure and magnetic properties of $\text{La}_3\text{Ni}_2\text{O}_7$ under pressure, arXiv:2309.17279 (2023).
- [34] S. N. Abadi *et al.*, Electronic structure of the alternating monolayer-trilayer phase of $\text{La}_3\text{Ni}_2\text{O}_7$, arXiv:2402.07143 (2024).
- [35] H. Li, X. Zhou, T. Nummy, J. Zhang, V. Pardo, W. E. Pickett, J. F. Mitchell, and D. S. Dessau, Fermiology and electron dynamics of trilayer nickelate $\text{La}_4\text{Ni}_3\text{O}_{10}$, Nat. Commun. **8**, 704 (2017).
- [36] J. Li *et al.*, Structural transition, electric transport, and electronic structures in the compressed trilayer nickelate $\text{La}_4\text{Ni}_3\text{O}_{10}$, Science China Physics, Mechanics & Astronomy **67**, 117403 (2024).
- [37] J. Zhang, H. Zheng, Y.-S. Chen, Y. Ren, M. Yonemura, A. Huq, and J. F. Mitchell, High oxygen pressure floating zone growth and crystal structure of the metallic nickelates $\text{R}_4\text{Ni}_3\text{O}_{10}$ ($\text{R}=\text{La},\text{Pr}$), Phys. Rev. Mater. **4**, 083402 (2020).
- [38] N. Yuan, A. Elghandour, J. Arneth, K. Dey, and R. Klingeler, High-pressure crystal growth and investigation of the metal-to-metal transition of Ruddlesden–Popper trilayer nickelates $\text{La}_4\text{Ni}_3\text{O}_{10}$, J. Cryst. Growth **627**, 127511 (2024).
- [39] J. Zhang *et al.*, Intertwined density waves in a metallic nickelate, Nat. Commun. **11**, 6003 (2020).
- [40] See Supplemental Material at [URL].
- [41] Z. Li, W. Guo, T. T. Zhang, J. H. Song, T. Y. Gao, Z. B. Gu, and Y. F. Nie, Epitaxial growth and electronic structure of Ruddlesden–Popper nickelates ($\text{La}_{n+1}\text{Ni}_n\text{O}_{3n+1}$, $n = 1-5$), APL Mater. **8**, 091112 (2020).
- [42] M.-C. Jung, J. Kapteghian, C. Hanson, B. Pamuk, and A. S. Botana, Electronic structure of higher-order Ruddlesden–Popper nickelates, Phys. Rev. B **105**, 085150 (2022).
- [43] Y. D. Li *et al.*, Ultrafast Dynamics of Bilayer and Trilayer Nickelate Superconductors, arXiv:2403.05012 (2024).
- [44] M. Kakoi *et al.*, Multiband Metallic Ground State in Multilayered Nickelates $\text{La}_3\text{Ni}_2\text{O}_7$ and $\text{La}_4\text{Ni}_3\text{O}_{10}$ Probed by ^{139}La -NMR at Ambient Pressure, J. Phys. Soc. Jpn. **93**, 053702 (2024).
- [45] J.-X. Wang, Z. Ouyang, R.-Q. He, and Z.-Y. Lu, Non-Fermi liquid and Hund correlation in $\text{La}_4\text{Ni}_3\text{O}_{10}$ under high pressure, Phys. Rev. B **109**, arXiv:2402.02581 (2024).
- [46] Z. Luo, C.-Q. Chen, M. Wang, W. Wú, and D.-X. Yao, Trilayer multi-orbital models of $\text{La}_4\text{Ni}_3\text{O}_{10}$, arXiv:2402.07196 (2024).
- [47] Y. Zhang, L.-F. Lin, A. Moreo, T. A. Maier, and E. Dagotto, Structural phase transition, $s\pm$ -wave

pairing, and magnetic stripe order in bilayered superconductor $\text{La}_3\text{Ni}_2\text{O}_7$ under pressure, Nat. Commun. **15**, arXiv:2307.15276 (2024).

[48] Y.-B. Liu, J.-W. Mei, F. Ye, W.-Q. Chen, and F. Yang, s_{\pm} -Wave Pairing and the Destructive Role of Apical-Oxygen Deficiencies in $\text{La}_3\text{Ni}_2\text{O}_7$ under Pressure, Phys. Rev. Lett. **131**, 236002 (2023).

[49] Y. Zhou *et al.*, Evidence of filamentary superconductivity in pressurized $\text{La}_3\text{Ni}_2\text{O}_7$ single crystals, arXiv:2311.12361 (2023).

[50] Z. Zhang, M. Greenblatt, and J. B. Goodenough, Synthesis, Structure, and Properties of the Layered Perovskite $\text{La}_3\text{Ni}_2\text{O}_{7-\delta}$, J. Solid State Chem. **108**, 402 (1994).